[10] C. M. Kudsia, "A generalized approach to the design and optimization of symmetrical microwave filters for communication systems," Ph.D. dissertation, Concordia Univer., Montreal, Canada, Nov. 1978.
[11] W. C. Tang, "A triple-mode six-pole elliptic function filter," M.A.Sc. Thesis, Faculty of Graduate Studies, Univer. Waterloo, Waterloo, Ont., Canada, Aug. 1983.
[12] S. B. Cohn, "Determination of aperture parameters by electrolytic-tank measurements," *Proc. IRE*, vol. 39, pp. 1416–1421, Nov. 1951.

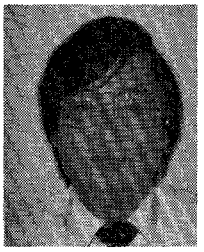

Wai-Cheung Tang (S'80–M'82) was born in Hong Kong, on November 20, 1953. He received the B.Sc. and M.Sc. degrees in electrical engineering from the University of Waterloo, Ont., Canada, in 1980 and 1983, respectively.

In 1980, he joined Com Dev. in Canada as a Microwave Engineer, where he is engaged in research and development on various types of filters and multiplexers for commercial satellite application. He is presently an Engineer Manager at Com Dev.

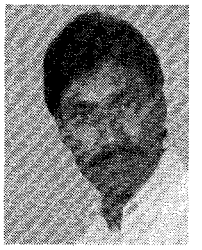

Sujeet K. Chaudhuri (M'79) was born in Calcutta, India, on Aug. 25, 1949. He received the B.E. (honors) degree in electronics engineering from the Birla Institute of Technology and Science, India, and the M. Tech. degree in electrical communication engineering from the Indian Institute of Technology, New Delhi, India, in 1970 and 1972, respectively. At the University of Manitoba Winnepeg, Man., Canada, he earned the M.Sc. degree in microwave engineering and the Ph.D. degree in electromagnetic theory in 1973 and 1977, respectively.

In 1977, he joined the University of Waterloo, Waterloo, Ont., Canada, where he is currently an Associate Professor in the Electrical Engineering Department. He has held Visiting Associate Professor's position in the University of Illinois, Chicago, during the years of 1981 and 1984. He has been involved in contractual research and consulting work with several Canadian industries and government research organizations. His current research interests are in electromagnetic scattering and diffraction with identification and imaging applications, impulse radar, and microwave components and integrated circuits.

Dr. Chaudhuri is a member of URSI Commission B, and Sigma Xi.

Accurate Hybrid-Mode Analysis of Various Finline Configurations Including Multilayered Dielectrics, Finite Metallization Thickness, and Substrate Holding Grooves

RÜDIGER VAHLDIECK

Abstract —**An accurate analysis of various finline configurations is introduced. The method of field expansion into suitable eigenmodes used considers the effects of finite metallization thickness as well as waveguide wall grooves to fix the substrate. Especially for millimeter-wave range applications, the propagation constant of the fundamental mode is found to be lower than by neglecting the finite thickness of metallization. For increasing groove depth in cases of asymmetrical and "isolated finline," higher order mode excitation reduces the monomode bandwidth significantly. In contrast to hitherto known calculations, this parameter only causes negligible influence on a fundamental mode if the groove depth is lower than half of the waveguide height.**

I. Introduction

MILLIMETER WAVE application of finline structures is of increasing importance for *E*-plane integrated circuit designs [1]–[5]. Real structure parameters, like finite metallization thickness, and waveguide grooves to fix the inset, considerably influence circuit behavior, especially in the higher frequency range. As for the metallization thickness, this influence has already been demonstrated by the example of low-insertion-loss finline and metal-insert filters [5], [6].

Hitherto known design theories [8], [11]–[18], however, widely neglect the influence of these parameters, and are considered, therefore, to yield appropriate finline circuit designs only for the lower frequency range. The unilateral earthed finline investigations by Beyer [19] reveal that both parameters have relatively high influence on fundamental mode behavior. In [19], the Ritz–Galerkin method is used and the continuity of the odd TE-mode field at the interfaces is applied as an example.

A comparison to the propagation constant of an idealized finline structure, given by Hofmann [9], seems to be in good agreement with [19] only when comparing finite strip thickness (70 μm) and zero groove depth or finite groove depth (0.326 mm) and zero strip thickness. It appears that this problem has not yet been solved completely as evi-

Manuscript received November 7, 1983; revised June 4, 1984.

The author was with the Microwave Department, University of Bremen, Federal Republic of Germany. He is now with the Department of Electrical Engineering, University of Ottawa, Ottawa, Ont., Canada K1N 6N5.

0018-9480/84/1100-1454$01.00 ©1984 IEEE

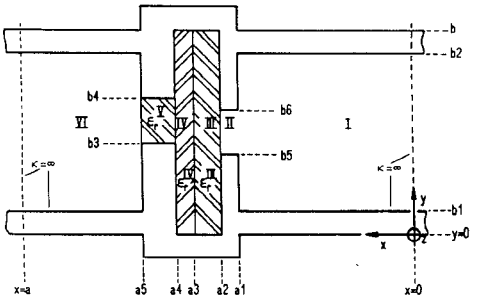

Fig. 1. Generalized finline structure with homogeneous and lossless dielectric in each subregion ($\mu_r = 1$).

denced by the absence of thorough investigation of higher order mode behavior with respect to the technologically conditioned circuit dimensions.

The purpose of this paper is to describe an accurate hybrid mode theory of a generalized finline configuration (Fig. 1) which includes finite strip thicknesses, substrate supporting grooves, asymmetric structures, and more than one dielectric region.

The higher order mode analysis presented utilized a generalized transverse-resonance relation which has already been successfully applied at microstrip structures [7] to reduce the size of the characteristic matrix equation considerably compared with the mode-matching technique in [10], [19]. In contrast to [19], the hybrid mode description used in this paper automatically involves the coupling of TE- and TM-waves. It will be shown that, only for finlines with homogeneous cross section ($\epsilon_r = 1$, ridged waveguide) or at cut-off frequencies both types of waves are decoupled. For the generalized case, therefore, inclusion of the TE- and TM-wave coupling effects on the field to be matched at the interfaces is necessary.

The transverse-resonance hybrid mode theory used in this paper yields a very efficient computer program to evaluate the normalized propagation constant. Numerical results are presented, especially for the E and T band and comparison with available results [4], [8]–[12], [14] establishes the accuracy of the numerical solutions in some special cases. In addition to the hybrid mode dispersion characteristics given, the effects due to finite metallization thickness and waveguide grooves are investigated in detail in order to provide design information for the practical choice of finline structural parameters.

II. Theory

The generalized finline structure given in Fig. 1 can be regarded as a transversal inhomogeneous parallel-plate line subdivided into partial homogeneous crossection ($\nu \epsilon$ I, II, III, IV, V, and VI). The electromagnetic field

$$\vec{E}^{(\nu)} = \nabla \times \nabla \times \vec{\prod}_e^{(\nu)} - j\omega\mu \nabla \times \vec{\prod}_m^{(\nu)} \tag{1}$$

$$\vec{H}^{(\nu)} = \nabla \times \nabla \times \vec{\prod}_m^{(\nu)} + j\omega\epsilon^{(\nu)} \nabla \times \vec{\prod}_e^{(\nu)} \tag{2}$$

in each subregion is expanded in an infinite series of eigenmodes and derived from the axial z components of the two independent vector potentials $\vec{\Pi}_m$ and $\vec{\Pi}_e$, which are assumed to be a sum of suitable eigenfunctions

$$\prod_{mz}^{(\nu)} = \sum_{n=0}^{\infty} fc_{(n)}^{(\nu)}(y) \cdot Im_{(n)}^{(\nu)}(x) \cdot e^{-jkz \cdot z} \tag{3}$$

$$\prod_{ez}^{(\nu)} = \sum_{n=1}^{\infty} fs_{(n)}^{(\nu)}(y) \cdot Ue_{(n)}^{(\nu)}(x) \cdot e^{-jkz \cdot z} \tag{4}$$

satisfying the boundary conditions and the scalar wave equation.

Considering the y-dependent boundary condition, the abbreviation $fs_{(n)}^{(\nu)}(y)$ and $fc_{(n)}^{(\nu)}(y)$ are given by

$$fc_{(n)}^{(\nu)}(y) = \frac{\cos k\tilde{y}_{(n)}^{(\nu)}}{\sqrt{1+\delta_{on}}}$$

$$fs_{(n)}^{(\nu)}(y) = \sin k\tilde{y}_{(n)}^{(\nu)}$$

$$k\tilde{y}_{(n)}^{(\nu)} = \frac{n \cdot \pi}{f^{(\nu)}} \cdot q^{(\nu)}$$

$$q^{(\nu)\prime} = [y - b_1, y - b_5, y, y, y - b_3, y - b_1]$$

$$f^{(\nu)\prime} = [b_2 - b_1, b_6 - b_5, b, b, b_4 - b_3, b_2 - b_1]$$

with the Kronecker delta δ_{on}. $Im_{(n)}^{(\nu)}(x)$ and $Ue_{(n)}^{(\nu)}(x)$ denote the partial wave amplitudes explained in the Appendix. The transverse resonance principle [7] is applied to reduce the size of the characteristic matrix equation for determining the normalized propagation constant kz/ko. For that reason, partial wave amplitudes

$$Im_{(n)}^{(\nu)}(x), Ue_{(n)}^{(\nu)}(x)$$

and

$$Ie_{(n)}^{(\nu)}(x) = \frac{1}{jkx_{(n)}^{(\nu)}} \frac{dUe_{(n)}^{(\nu)}(x)}{dx}$$

$$Um_{(n)}^{(\nu)}(x) = \frac{dIm_{(n)}^{(\nu)}(x)}{dx}$$

summarized as vectors $\boldsymbol{U}^{(\nu)}$ and $\boldsymbol{I}^{(\nu)}$ at the left-side boundary ($x = xo$) of each subregion (ν) are determined by the amplitudes of its right-side boundary ($x = xu$). The transfer matrix $\boldsymbol{R}^{(\nu)}$ gives the relation between $\boldsymbol{I}^{(\nu)}$ and $\boldsymbol{U}^{(\nu)}$ at the two coordinates in the following manner

$$\underset{(x=xo)}{\begin{bmatrix} \boldsymbol{U}^{(\nu)} \\ \boldsymbol{I}^{(\nu)} \end{bmatrix}} = \underbrace{\begin{bmatrix} \boldsymbol{Rc}^{(\nu)} & \boldsymbol{Rs}^{(\nu)} \\ \boldsymbol{Rs}^{(\nu)\prime} & \boldsymbol{Rc}^{(\nu)} \end{bmatrix}}_{\boldsymbol{R}^{(\nu)}} \cdot \underset{(x=xu)}{\begin{bmatrix} \boldsymbol{U}^{(\nu)} \\ \boldsymbol{I}^{(\nu)} \end{bmatrix}} \tag{5}$$

with the diagonal matrices $\boldsymbol{Rc}^{(\nu)}$, $\boldsymbol{Rs}^{(\nu)}$, and $\boldsymbol{Rs}^{(\nu)\prime}$ given in the Appendix.

To satisfy the continuity condition at each common interface, modified continuity equations lead to the follow-

ing expressions

$$Ey: \quad \frac{\partial \Pi_{mz}^{(\nu+1)}}{\partial x} = \frac{\partial \Pi_{mz}^{(\nu)}}{\partial x} - K_{\mu}^{(\nu)}(\omega, kz)\frac{\partial \Pi_{ez}^{(\nu)}}{\partial y} \tag{6}$$

$$Ez: \quad \Pi_{ez}^{(\nu+1)} = K^{(\nu)}(\omega, kz)\Pi_{ez}^{(\nu)} \tag{7}$$

$$Hz: \quad \Pi_{mz}^{(\nu+1)} = K^{(\nu)}(\omega, kz)\Pi_{mz}^{(\nu)} \tag{8}$$

$$Hy: \quad \frac{\partial \Pi_{ez}^{(\nu+1)}}{\partial x} = \frac{\epsilon_r^{(\nu)}}{\epsilon_r^{(\nu+1)}} \cdot \frac{\partial \Pi_{ez}^{(\nu)}}{\partial x} + K_{\epsilon}^{(\nu)}(\omega, kz)\frac{\partial \Pi_{mz}^{(\nu)}}{\partial y} \tag{9}$$

with

$$K^{(\nu)}(\omega, kz) = \frac{\epsilon_r^{(\nu)} - (kz/ko)^2}{\epsilon_r^{(\nu+1)} - (kz/ko)^2}$$

$$K_{\mu}^{(\nu)}(\omega, kz) = \frac{kz}{\omega\mu}\left(1 - K^{(\nu)}(\omega, kz)\right)$$

for $K_{\epsilon}^{(\nu)}(\omega, kz)$ replace $\epsilon_o \cdot \epsilon_r^{(\nu+1)}$ by μ.

The coupling between TE and TM waves is automatically involved in (6)–(9). Only in cases of finline configurations with homogeneous cross-sectional propagation media (e.g., ridged waveguide) or at cut-off frequency ($kz/ko = 0$), both types of waves are decoupled since $K\mu^{(\nu)}(\omega, kz)$ and $K\epsilon^{(\nu)}(\omega, kz)$ vanish.

The left-side $(\nu+1)$ x-dependent partial wave amplitudes in (6)–(9) are separated by multiplying with appropriate orthogonal functions which lead directly to the transition matrix $\boldsymbol{V}^{(\nu)}$ of each interface section and hence combine the adjacent amplitude vectors $\boldsymbol{I}^{(\nu)}$ and $\boldsymbol{I}^{(\nu+1)}$ as well as $\boldsymbol{U}^{(\nu)}$ and $\boldsymbol{U}^{(\nu+1)}$

$$\begin{bmatrix} \boldsymbol{Um}^{(\nu+1)} \\ \boldsymbol{Ue}^{(\nu+1)} \\ \boldsymbol{Im}^{(\nu+1)} \\ \boldsymbol{Ie}^{(\nu+1)} \end{bmatrix}_{(x=a_\nu)} = \underbrace{\begin{bmatrix} \tilde{y}^{(\nu)}\boldsymbol{ec}^{(\nu)} & -\tilde{y}^{(\nu)}K_{\mu}^{(\nu)}(\omega, kz)\tilde{\boldsymbol{ec}}^{(\nu)} & \boldsymbol{0} & \boldsymbol{0} \\ \boldsymbol{0} & \tilde{y}^{(\nu)}K^{(\nu)}(\omega, kz)\tilde{\boldsymbol{es}}^{(\nu)} & \boldsymbol{0} & \boldsymbol{0} \\ \boldsymbol{0} & \boldsymbol{0} & \bar{y}^{(\nu)}K^{(\nu)}(\omega, kz)\bar{\boldsymbol{ec}}^{(\nu)} & \boldsymbol{0} \\ \boldsymbol{0} & \boldsymbol{0} & -K_{\epsilon}^{(\nu)}(\omega, kz)\tilde{\boldsymbol{es}}^{(\nu)} & \bar{y}^{(\nu)}\dfrac{\epsilon_r^{(\nu)}}{\epsilon_r(\nu+1)}\boldsymbol{es}^{(\nu)} \end{bmatrix}}_{\boldsymbol{V}^{(\nu)}} \cdot \begin{bmatrix} \boldsymbol{Um}^{(\nu)} \\ \boldsymbol{Ue}^{(\nu)} \\ \boldsymbol{Im}^{(\nu)} \\ \boldsymbol{Ie}^{(\nu)} \end{bmatrix}_{(x=a_\nu)} . \tag{10}$$

The abbreviations are explained in the Appendix.

Successively applying the transfer matrix $\boldsymbol{R}^{(\nu)}$ to the corresponding transition matrix $\boldsymbol{V}^{(\nu)}$ finally leads to a relation between amplitude vectors at the left $(x = a)$ and the right boundary $(x = 0)$

$$\begin{bmatrix} \boldsymbol{U}^{(\mathrm{VI})} \\ \boldsymbol{I}^{(\mathrm{VI})} \end{bmatrix}_{(x=a)} = \underbrace{\boldsymbol{R}^{(\mathrm{VI})} \cdot \prod_{\nu=\mathrm{V}}^{\nu=\mathrm{I}} \boldsymbol{V}^{(\nu)} \cdot \boldsymbol{R}^{(\nu)}}_{\boldsymbol{G}} \begin{bmatrix} \boldsymbol{U}^{(\mathrm{I})} \\ \boldsymbol{I}^{(\mathrm{I})} \end{bmatrix}_{(x=0)} . \tag{11}$$

For the numerical solution, the infinite set of equations for $\boldsymbol{U}_L$ and $\boldsymbol{I}_L$ is truncated by the end index $L = 2N-1$; so, the matrix size of $\boldsymbol{G}$ is of order $4N-2$ and keeps constant, even for an increasing number of discontinuities. If N is the number of summation terms in (3) and (4) for all investigated finline structures, a maximum of $N = 17$ has turned out to be sufficient.

The transverse resonance relation requires the boundary conditions at the metallic surface $x = 0$, $x = a$ (Fig. 1), to be considered now. With respect to the relation $\boldsymbol{U} \sim \boldsymbol{0}$, consequently the characteristic matrix equation is reduced to the upper right quarter of the matrix product in (11)

$$\begin{bmatrix} \boldsymbol{0} \\ \boldsymbol{0} \end{bmatrix}_{(x=a)} = \begin{bmatrix} \boldsymbol{G}_{12}^{hh} & \boldsymbol{G}_{12}^{he} \\ \boldsymbol{G}_{12}^{eh} & \boldsymbol{G}_{12}^{ee} \end{bmatrix} \cdot \begin{bmatrix} \boldsymbol{Im}^{(\mathrm{I})} \\ \boldsymbol{Ie}^{(\mathrm{I})} \end{bmatrix}_{(x=0)} . \tag{12}$$

$\boldsymbol{G}_{12}$ is of size $2N-1$ and the zeros of the determinant

$$\det(\boldsymbol{G}_{12}) = 0 \tag{13}$$

which is a transcendent function of

$$kx_{(n)}^{(\nu)} = ko\sqrt{\epsilon_r^{(\nu)} - \left(\frac{n \cdot \pi}{f^{(\nu)} \cdot ko}\right)^2 - \left(\frac{kz}{ko}\right)^2} \tag{14}$$

$$ko = \omega\sqrt{\mu_o \epsilon_o}$$

provide the desired dispersion characteristic.

III. Results

Dispersion characteristics of the dominant and first higher order modes are given in Fig. 2 for the bilateral finline. The structure shielded by a *Ka*-band waveguide has the same dimensions as that used by Hofmann [8] and Schmidt [12]. Considering finite thickness of metallization ($t1 = t2 = 1$ μm) and a dielectric between the fins ($\epsilon_r^{\mathrm{V}} = 3.0 = \epsilon_r^{\mathrm{II}}$, see Fig. 1), results are in good agreement with these authors. Without a slot dielectric ($\epsilon_r^{\mathrm{V}} = \epsilon_r^{\mathrm{II}} = 1.0$), however, evaluated data are 3 percent less, on the average. This discrepancy can be explained by the fact that, due to an infinitely thin metallization [8], [12], the field between the fins is mainly concentrated within the dielectric and thus causes a higher value of propagation constant.

In order to demonstrate the fundamental mode behavior in finlines with considerable metallization thickness at 75 GHz (Fig. 3(a)), unilateral and bilateral finlines with thin substrates are considered. In the case of a bilateral finline with relatively thick substrate in a *T*-band waveguide mount (Fig. 3(b)), the influence of the finite strip thickness on the fundamental mode is smaller and deviations from values with negligible strip thickness given in [4] are not as high as expected in view of Fig. 3(a).

Fig. 4 shows the influence of the groove depth e on the propagation constant for the unilateral finline centered in the waveguide (*E* band). Comparing the results with Beyer [19] and using his definition of ϵ_{eff}, which gives a relation between the cut-off wavelength of an equivalent air-filled

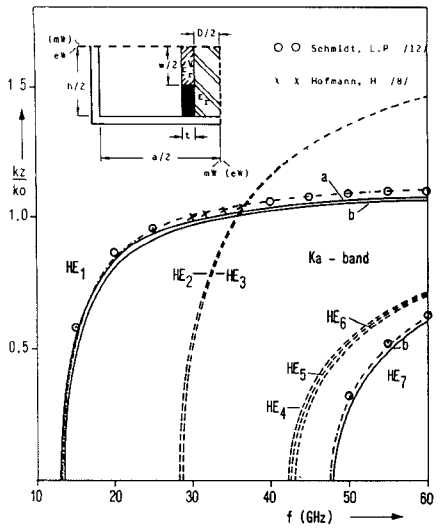

Fig. 2. Dispersion characteristic of a bilaterial finline (eW: electric wall, mw: magnetic wall; $a = 7.112$ mm, $h = a/2$; $\epsilon_r = 3.0$; $D = 125$ μm; $w = 0.5$ mm; (- · · · · · -) $t = 1.0$ μm, $\epsilon_r^V = 3.0$; (———)$\epsilon_r^V = 1.0$, a: $t = 5$ μm, b: $t = 1$ μm; (----) nonexcited modes, $t = 1.0$ μm, groove depth $e = 0$).

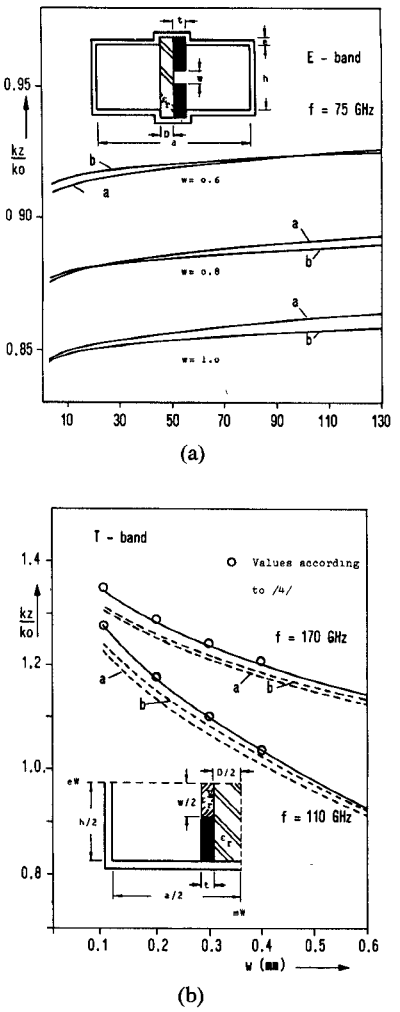

Fig. 3. (a) Fundamental mode (HE_1) versus the metallization thickness $t(\mu m)$ in a unilateral finline b with several slot widths w(mm). a a bilateral finline for comparison ($a = 3.1$ mm, $h = a/2$; $D = 50$. μm, $\epsilon_r = 3.0$, $e = 0.326$ mm). (b) Fundamental mode (HE_1) versus the slot width in a bilateral finline ($a = 1.65$ mm, $h = a/2$; $D = 110$ μm, $\epsilon_r = 3.75$; $e = 0$; (———) $t = 0.5$ μm, $\epsilon_r^V = 3.75$; (----)$\epsilon_r^V = 1.0$, a: $t = 0.5$ μm, b: $t = 5$ μm).

ridged waveguide and the finline wavelength at 75 GHz, the disagreement is significant (Fig. 4(a)). Since the field is concentrated mainly in the slots, one expects that the depth of the grooves has only a minor influence on the dominant mode. This fact has been confirmed with the present method for all investigated finlines with various slot widths and groove depths lower than half of the waveguide height. However, the second-order mode propagation which limits the practically most interesting monomode range is highly influenced. This behavior is illustrated in Fig. 4(b) containing the bandwidth which is a ratio of the nearly constant first cut-off wavelength λ_{C1} and the next higher mode cut-off wavelength λ_{C2} versus the groove depths. Although the first higher order mode for the bilateral finline reveals the highest dependence on groove depth, this mode is not excited by an H_{10}-wave of the empty waveguide. In contrast to other finline structures, the next excitable higher order mode (HE_7, Fig. 2) indicates a negligible influence on groove depth. So, this configuration provides the highest monomode range. If the grooves are deeper than half of the waveguide height, for a unilateral finline with the same dimension given in Fig. 3(b), Fig. 4(c) shows an obvious interaction between the fundamental and second higher order mode and results in a significant deviation of dispersion characteristics (Fig. 5) from those given in [4]. This interaction effect is also evident for a generalized finline structure with multilayered dielectrics and different metallization thicknesses (Fig. 6). This structure obviously reveals the necessity to consider all important higher order modes.

Similar observations are possible in other asymmetrical configurations, but will be of minor interest for small substrate thicknesses with low dielectric constant and small groove depths related to the waveguide height. This is demonstrated (Fig. 7) for an antipodal finline with nonoverlapping fins. The bandwidth behavior, as well as the dispersion characteristic, resembles somewhat that of a comparable unilateral structure, but all higher order modes are excited.

Modal dispersion curves of a so-called "isolated finline" are presented in Fig. 8. In practical applications for active components, one or both fins are isolated by a gasket which allows a dc voltage to be developed across the fins. RF continuity between the fins and the waveguide wall is achieved by using a choke section of a quarter wavelength groove in the waveguide broadwall at center frequency. Neglecting the groove as well as the finite metallization thickness shows a good agreement with the cut-off wavelength obtainable from [14]. In practical realization, however, this configuration provides TEM behavior which is also neglected in [14], [16] and leads to a somewhat different theoretical procedure.

Furthermore, it should be noticed that, in contrast to the unilateral and antipodal finline, where the next excitable higher order modes result originally from the H_{2o}-, respec-

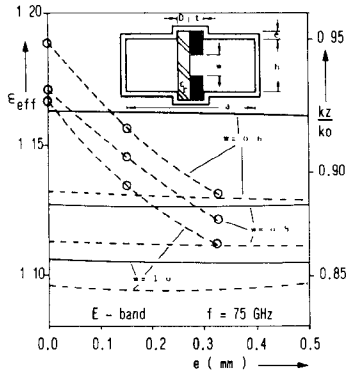

(a)

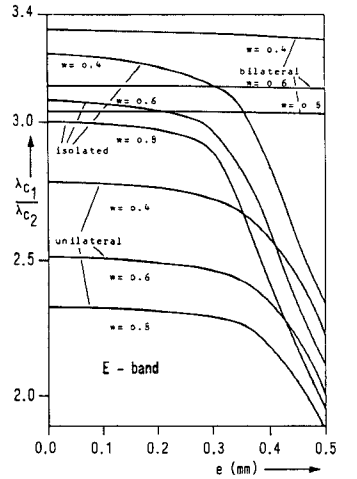

(b)

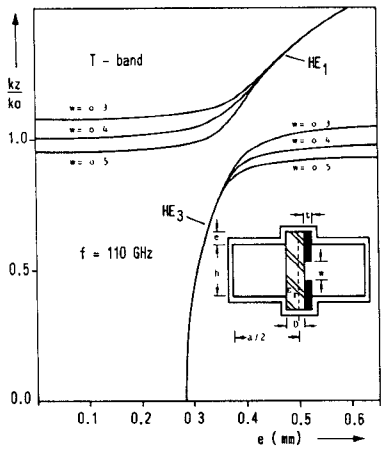

(c)

Fig. 4. (a) Fundamental mode (HE_1) versus the groove depths e in a unilateral finline with several slot widths w(mm) ($a = 3.1$ mm, $h = a/2$; $D = 50.0$ μm, $\epsilon_r = 3.0$, $t = 70.0$ μm)

$\circ\circ\circ$ values according to [19] $\Big\}\ \epsilon_{\text{eff}} = \lambda_0^2\left(\frac{1}{\lambda_g^2} + \frac{1}{\lambda_c^2}\right)$

λ_0—free space wavelength, λ_g—finline wavelength (75 GHz), λ_c—cutoff wavelength of an equivalent ridge waveguide. (———) normalized phase constant kz/ko). (b) Monomode bandwidth for a bilateral, unilateral and isolated finline with several slot widths. For the isolated finline $D/2 = 25.0$ μm (see the structure in Fig. 8) (λc_1: cutoff-wavelength of the dominant mode, λc_2: cutoff-wavelength of the next higher order mode excited by an incident H_{10}-wave). (c) Normalized phase constant versus the groove depth in a unilateral structure with several slot widths ($a = 1.65$ mm, $h = a/2$; $D = 110.0$ μm, $\epsilon_r = 3.75$, $t = 5.0$ μm).

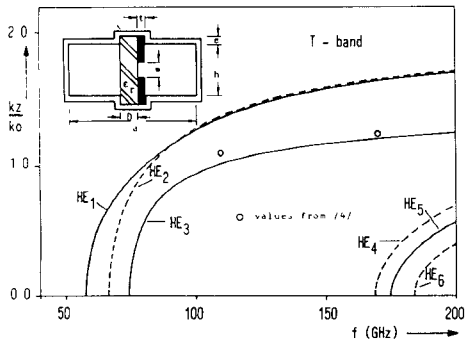

Fig. 5. Dispersion characteristic for the first six eigenmodes in a unilateral finline $w = 0.3$ mm, $e = 0.5$ mm, all other dimensions according to Fig. 4(c). (----) these modes are not excited by an incident H_{10}-wave.

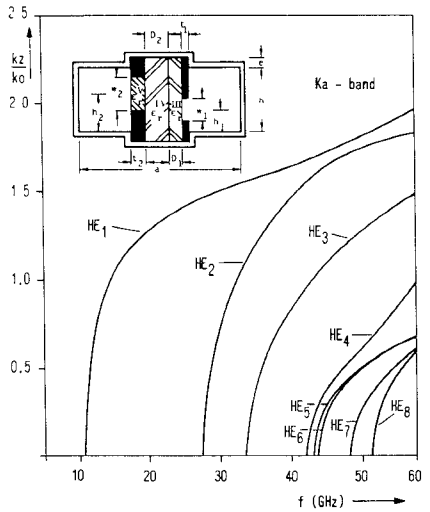

Fig. 6. Dispersion characteristic of an asymmetrical bilateral finline in the Ka = band range ($a = 7.112$ mm, $h = a/2$, $h1 = 1.0$ mm, $h2 = 2.0$ mm; $D1 = 125.0$ μm, $\epsilon_r^{III} = 3.0$, $D2 = 254.0$ μm, $\epsilon_r^{IV} = 9.6$, $\epsilon_r^{V} = 3.75$; $t1 = 10.0$ μm, $t2 = 50.0$ μm; $w1 = 1.5$ mm, $w2 = 2.5$ mm; $e = 0.5$ mm).

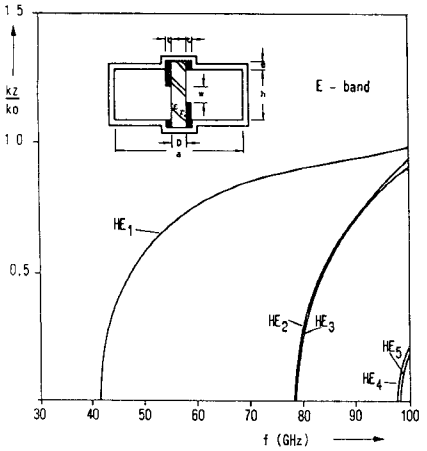

Fig. 7. Dispersion characteristic of the first five eigenmodes in an antipodal finline ($a = 3.1$ mm, $h = a/2$; $D = 50.0$ μm, $\epsilon_r = 3.0$; $t = 10.0$ μm; $w = 0.8$ mm; $e = 0.5$mm).

tively, H_{o1}-mode of the empty waveguide, the HE_4-mode in Fig. 8 results originally from the H_{3o}-mode and shows a high dependency on groove depth (Fig. 4(b)) which is not observed for the same mode in the case of a symmetric bilateral finline.

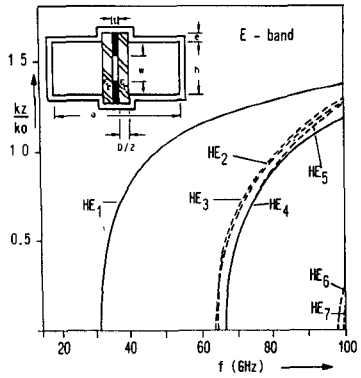

Fig. 8. Dispersion characteristic of an isolated finline ($a = 3.1$ mm, $h = a/2$; $D = 220.0$ μm, $\epsilon_r = 3.75$; $w = 0.6$ mm; $t = 5.0$ μm; $e = 0.5$ mm).

Finally, it must be emphasized that, for all these finline modes, the field distribution differs widely from those of an empty waveguide. The computation time for most symmetrical structures is 1–2 s, on the average, on a Siemens 7880. This corresponds to a 0.5- percent accuracy in the calculation of one phase constant for one frequency sample point.

IV. Conclusion

A method has been described which allows an accurate analysis of various finline structures, including all important parameters of real dimensions. Comparison between often used finline configurations indicates that the bilateral finline behaves best and provides the largest monomode bandwidth due to its virtual insensitivity to the groove depth. In asymmetrical structures, higher order modes cut-off frequencies are considerably reduced by the depth of the groove, which is much more critical than the strip thickness. Hence, it follows that, at high frequencies, the grooves supporting the substrate cannot be neglected and their influence is more significant than the effect of finite metallization thickness.

Appendix I

Abbreviations for the partial wave amplitudes in (3) and (4)

$$Im_{(n)}^{(\nu)}(x) = A_{(n)}^{(\nu)} e^{jkx_{(n)}^{(\nu)} \cdot x_a} + B_{(n)}^{(\nu)} e^{-jkx_{(n)}^{(\nu)} \cdot x_a}$$

$$Ue_{(n)}^{(\nu)}(x) = \frac{1}{jkx_{(n)}^{(\nu)}} \left(C_{(n)}^{(\nu)} e^{jkx_{(n)}^{(\nu)} \cdot x_a} - D_{(n)}^{(\nu)} e^{-jkx_{(n)}^{(\nu)} \cdot x_a} \right)$$

$$x_a = xo - xu$$

and for the diagonal matrices in (5)

$$\boldsymbol{Rc}_{(n)}^{(\nu)} = \begin{bmatrix} \cosh\left(jkx_{(n)}^{(\nu)} \cdot x_a\right) & 0 \\ 0 & \cosh\left(jkx_{(n)}^{(\nu)} \cdot x_a\right) \end{bmatrix}$$

$$\boldsymbol{Rs}_{(n)}^{(\nu)} = \begin{bmatrix} jkx_{(n)}^{(\nu)} \sinh\left(jkx_{(n)}^{(\nu)} \cdot x_a\right) & 0 \\ 0 & \frac{1}{jkx_{(n)}^{(\nu)}} \sinh\left(jkx_{(n)}^{(\nu)} \cdot x_a\right) \end{bmatrix}$$

$$\boldsymbol{Rs}_{(n)}^{(\nu)\prime} = \begin{bmatrix} \frac{1}{jkx_{(n)}^{(\nu)}} \sinh\left(jkx_{(n)}^{(\nu)} \cdot x_a\right) & 0 \\ 0 & jkx_{(n)}^{(\nu)} \sinh\left(jkx_{(n)}^{(\nu)} \cdot x_a\right) \end{bmatrix}.$$

Appendix II

Abbreviations in the transition matrix equation (10)

$$\tilde{y}^{(\nu)\prime} = \left[\frac{b_2 - b_1}{2}, \frac{2}{b}, 1, \frac{b}{2}, \frac{2}{b_1 - b_2} \right]$$

$$\bar{y}^{(\nu)\prime} = \left[\frac{2}{b_6 - b_5}, \frac{b_6 - b_5}{2}, 1, \frac{2}{b_4 - b_3}, \frac{b_4 - b_3}{2} \right]$$

$$\tilde{ec}^{(\nu)} = \begin{cases} \boldsymbol{Fc}^{(\mathrm{II})} \cdot \boldsymbol{p} \cdot \dfrac{1}{b_6 - b_5} \\ \boldsymbol{E} \cdot \boldsymbol{p} \cdot \dfrac{1}{b} \\ \left(\boldsymbol{Fc}^{(\mathrm{IV})}\right)^{-1} \cdot \boldsymbol{p} \cdot \dfrac{1}{2} \\ \boldsymbol{Fc}^{(\mathrm{V})} \cdot \boldsymbol{p} \cdot \dfrac{1}{b_2 - b_1} \end{cases}$$

$$\tilde{es}^{(\nu)} = \begin{cases} \left(\boldsymbol{Fs}^{(\mathrm{II})T}\right)^{-1} \cdot \boldsymbol{p} \cdot \dfrac{1}{2} \\ \boldsymbol{E} \cdot \boldsymbol{p} \cdot \dfrac{1}{b} \\ \boldsymbol{Fs}^{(\mathrm{IV})^T} \cdot \boldsymbol{p} \cdot \dfrac{1}{b} \\ \boldsymbol{Fs}^{(\mathrm{V})^T} \cdot \boldsymbol{p} \cdot \dfrac{1}{2} \end{cases}$$

where $\tilde{es}^{(\nu)}$ receives an additional zero column, $\boldsymbol{p}$ is the diagonal matrix with the elements $i \cdot \pi$ $(i = 1,2,3 \cdots, N)$, and $\boldsymbol{Fc}^{(\nu)}$, $\boldsymbol{Fs}^{(\nu)}$ are the coupling integrals

$$\boldsymbol{Fc}_{(n,i)}^{(\mathrm{I})} = \int_{y=b_5}^{y=b_6} fc_{(n)}^{(\mathrm{I})}(y) \cdot fc_{(i)}^{(\mathrm{II})}(y)\, dy$$

$$\boldsymbol{Fc}_{(n,i)}^{(\mathrm{II})} = \int_{y=b_5}^{y=b_6} fc_{(n)}^{(\mathrm{III})}(y) \cdot fc_{(i)}^{(\mathrm{II})}(y)\, dy$$

$$\boldsymbol{Fc}_{(n,i)}^{(\mathrm{III})} = \int_{y=b_3}^{y=b_4} fc_{(n)}^{(\mathrm{IV})}(y) \cdot fc_{(i)}^{(\mathrm{V})}(y)\, dy$$

$$\boldsymbol{Fc}_{(n,i)}^{(\mathrm{IV})} = \int_{y=b_3}^{y=b_4} fc_{(n)}^{(\mathrm{VI})}(y) \cdot fc_{(i)}^{(\mathrm{V})}(y)\, dy.$$

For the coupling integrals $\boldsymbol{Fs}^{(\nu)}$, replace $fs^{(\nu)}(y)$ instead of $fc^{(\nu)}(y)$

$$\boldsymbol{ec}^{(\nu)} = \begin{cases} \left(\boldsymbol{Fc}^{(\mathrm{I})}\right)^{-1} \\ \boldsymbol{Fc}^{(\mathrm{II})} \\ \boldsymbol{E} \\ \left(\boldsymbol{Fc}^{(\mathrm{IV})}\right)^{-1} \\ \boldsymbol{Fc}^{(\mathrm{V})} \end{cases} \qquad \boldsymbol{es}^{(\nu)} = \begin{cases} \boldsymbol{Fs}^{(\mathrm{I})^T} \\ \left(\boldsymbol{Fs}^{(\mathrm{II})^T}\right)^{-1} \\ \boldsymbol{E} \\ \boldsymbol{Fs}^{(\mathrm{IV})^T} \\ \left(\boldsymbol{Fs}^{(\mathrm{V})^T}\right)^{-1} \end{cases}$$

$$\bar{\boldsymbol{ec}}^{(\nu)} = \begin{cases} \boldsymbol{Fc}^{(\mathrm{I})T} \\ \left(\boldsymbol{Fc}^{(\mathrm{II})^T}\right) - 1 \\ \boldsymbol{E} \\ \boldsymbol{Fc}^{(\mathrm{IV})^T} \\ \left(\boldsymbol{Fc}^{(\mathrm{V})^T}\right)^{-1} \end{cases} \qquad \bar{\boldsymbol{es}}^{(\nu)} = \begin{cases} \left(\boldsymbol{Fs}^{(\mathrm{I})}\right)^{-1} \\ \boldsymbol{Fs}^{(\mathrm{II})} \\ \boldsymbol{E} \\ \left(\boldsymbol{Fs}^{(\mathrm{IV})}\right)^{-1} \\ \boldsymbol{Fs}^{(\mathrm{V})} \end{cases}.$$

where $\boldsymbol{E}$ denotes the unit matrix.

ACKNOWLEDGMENT

The author wishes to thank Prof. Dr.-Ing. F. Arndt who supported this work with helpful discussions.

REFERENCES

[1] P. T. Meier, "Integrated fin-line millimeter components," *IEEE Trans. Microwave Theory Tech.*, vol. MTT-22, pp. 1209–1216, Dec. 1974.

[2] P. T. Meier "Millimeter integrated circuits suspended in the *E*-plane of rectangular waveguides," *IEEE Trans. Microwave Theory Tech.*, vol. MTT-26, pp. 726–733, Oct. 1978.

[3] R. N. Bates, S. J. Nightingale, and P. M. Ballard, "Millimeter-wave *E*-plane components and subsystems," *Radio Electron. Eng.*, vol. 57, pp. 506–512, Nov./Dec., 1982.

[4] B. Adelseck, H. Callsen, H. Hofmann, H. Meinel, and B. Rembold, "Neue millimeterwellenkomponenten in quasiplanarer leitungstechnik," *Frequenz*, vol. 35, pp. 118–123, 1981.

[5] F. Arndt, J. Bornemann, D. Grauerholz, and R. Vahldieck, "Theory and design of low-insertion loss fin-line filter," *IEEE Trans. Microwave Theory Tech.*, vol. MTT-30, pp. 155–163, Feb. 1982.

[6] R. Vahldieck, J. Bornemann, F. Arndt, and D. Grauerholz, "Optimized waveguide *E*-plane metal insert filters for millimeter-wave applications," *IEEE Trans. Microwave Theory Tech.*, vol. MTT-31, pp. 65–69, Jan. 1983.

[7] F. Arndt and G. U. Paul, "The reflection definition of the characteristic impedance of microstrips," *IEEE Trans. Microwave Theory Tech.*, vol. MTT-27, pp. 724–731, Aug. 1979.

[8] H. Hofmann, "Dispersion of planar waveguides for millimeter-wave application," *Arch. Elek. Übertragung*, vol. 31, pp. 40–44, 1977.

[9] H. Hofmann, H. Meinel, and B. Adelseck, "Möglichkeiten der Integration von Millimeter-Wellen-Komponenten," *Nachrichtentechn. Zeitschrift (NTZ)*, vol. 31, pp. 752–757, 1978.

[10] J. Siegel, "Phasenkonstante und Wellenwiderstand einer Schlitzleitung mit rechteckigem Schirm und endlicher Metallisierungsdicke," *Frequenz*, vol. 31, pp. 216–220, July 1977.

[11] J. Siegel "Grundwelle und höhere wellentypen bei fin-leitungen," *Frequenz*, vol. 34, pp. 196–200, July 1980.

[12] L.-P. Schmidt and T. Itoh, "Spectral domain analysis of dominant and higher order modes in fin-lines," *IEEE Trans. Microwave Theory Tech.*, vol. MTT-28, pp.981–985, Sept. 1980.

[13] L.-P. Schmidt, T. Itoh, and H. Hofmann, "Characteristics of unilateral fin-line structures with arbitrarily located slots," *IEEE Trans. Microwave Theory Tech.*, vol. MTT-29, pp. 352–355, Apr. 1981.

[14] Y.-C. Shih and W. J. R. Hoefer, "Dominant and second-order mode cutoff frequencies in fin-lines calculated with a two-dimensional TLM program," *IEEE Trans. Microwave Theory Tech.*, vol. MTT-24, pp. 1443–1448, Dec. 1980.

[15] A. K. Sharma and W. J. R. Hoefer, "Empirical expression for fin-line design," *IEEE Trans. Microwave Theory Tech.*, vol. MTT-31, pp. 350–356, Apr. 1983.

[16] A. M. K. Saad and G. Begemann, "Electrical performance of fin-lines of various configuration," *Microwaves, Opt. Acoust.*, vol. 1, no. 2, pp. 81–88, Jan. 1977.

[17] A. M. K. Saad and K. Schünemann, "A simple method for analyzing fin-line structures," *IEEE Trans. Microwave Theory Tech.*, vol. MTT-26, pp. 1007–1011, Dec. 1978.

[18] A. M. K. Saad and K. Schünemann, "Efficient eigenmode analysis for planar transmission lines," *IEEE Trans. Microwave Theory Tech.*, vol. MTT-30, pp. 2125–2132, Dec. 1982.

[19] A. Bayer, "Analysis of the characteristics of an earthed fin-line," *IEEE Trans. Microwave Theory Tech.*, vol. MTT-29, pp. 676–680, July 1981.

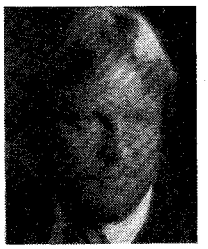

Rüdiger Vahldieck was born in Heiligenhafen, West Germany, in 1951. He received the Dipl.-Ing. and the Dr.-Ing. degrees, both in electrical engineering, from the University of Bremen, Bremen, West Germany, in 1980 and 1983, respectively. His Dr.-Ing. thesis was on the numerical analysis of generalized finline configurations and the design and development of low insertion loss finline filters.

From 1980–1983, he was a Research Assistant at the Microwave Department of the University of Bremen where he was engaged in computer-aided design of millimeter-wave integrated circuits. Since 1984, he has been a Post-Doctoral Fellow at the University of Ottawa, Ottawa, Canada. His research activities at present have chiefly been concerned with broadband millimeter-wave couplers and different numerical techniques to solve electromagnetic field problems in finline structures.

Dr. Vahldieck is one of the recipients of the A. F. Bulgin Premium of the Institution of Electronic and Radio Engineers, 1983.